DOI: 10.15480/882.9304

Eighth International Symposium on Marine Propulsors
smp'24, Berlin, Germany, March 2024

Design Exploration Study with Counter-Rotating Propellers for a Zero-Emission Coaster Vessel

Vladimir Krasilnikov[1]

[1]Norwegian Marine Technology Research Institute (SINTEF Ocean), Trondheim, Norway

ABSTRACT

This paper describes a simulation driven approach to the design of a shaft counter-rotating propeller (CRP) system for the next generation coaster vessel. The design workflow involves parametric CAD models of ship hull, propellers and rudder, and numerical tools of different fidelity levels which are employed in exploration studies, iterative elaboration of propeller design and final verification of ship's propulsion performance. It is demonstrated that, in the present case, with a wake-adapted CRP design one can achieve a power reduction of 8.5 to 9.0 % compared to the solution with a single propeller designed for the same conditions. In addition to propulsion characteristics, the paper also presents the analysis of unsteady loads on propeller blades and rudder, propeller-induced pressure pulses on the hull and radiated noise level, comparing the mentioned quantities between the CRP and single propeller designs.

Keywords

Ship propulsion, Energy efficiency, Counter-rotating propellers, CFD, Simulation driven design.

1 INTRODUCTION

In the quest for improving ship's propulsion efficiency, coaxial counter-rotating propellers (CRP) present an attractive and proven solution. CRP boast a highly successful history in aviation (Flippone 2023). However, the original concept and its first full-scale trials are found in marine propulsion applications due to the works by Ericsson in 1836 and de Bay in 1876 (Carlton 2007). By virtue of natural compensation of torque reaction by propellers rotating in opposite directions, CRP are widely used on torpedoes and small outboard motors. The main principle of recovering rotational energy in the slipstream of the forward propeller makes CRP applicable for a broad range of ship types and loading conditions. According to Mewis (2014), power reduction of 5 to 14 % is achievable with CRP in the range of thrust loading coefficient, CTh, from 0.5 to 5.0, where higher savings correspond to conditions of heavier loading. Such a performance is superior to all other hydrodynamic energy saving devices currently installed on ships. Another advantage is the possibility to distribute the required thrust load between the two propellers, and hence increase the cavitation margin. However, higher production and maintenance costs and a greater complexity of the shafting system have, until recently, hindered wide installation of shaft CRP on seagoing merchant ships, with the notable exceptions of IHI CRP designs for the 37000 dwt bulk carrier JUNO in 1988, and for the 259000 dwt VLCC OKINOSHIMA-MARU in 1993 in Japan (IHI, 1993). Instead, CRP solutions involving azimuth pod units have been developed, including hybrid CRP systems (Ueda et al. 2004; Quereda et al. 2019) and pure podded units featuring either pushing CRP (ITTC 2008) or twin pushing/pulling CRP (Jukola & Ronkainen 2006). In recent years, the interest in shaft CRP has returned thanks to the innovations in shaft-in-shaft technology, and improvements in outboard shaft seals, shaft bearings and lubrication system (Ship Technology 2014).

In this paper we describe a multi-fidelity workflow employed in the design of a shaft CRP system for the next generation of zero-emission coaster vessels. The said workflow is based on the parametric models of propulsor, rudder and ship hull, and software connections built in the CAE platform CAESES. It involves the in-house propeller design suite AKPA by SINTEF Ocean as well as the commercial CFD code STAR-CCM+, which are used at different stages of the design process to ensure accurate adaptation of propulsor to operation conditions behind ship hull. To provide an adequate quantification of power savings achievable with CRP, CFD self-propulsion simulations are conducted in full scale for the ship equipped with the designed CRP system and with a single propeller, which is designed for the same operation conditions. Further, we address such less studied questions as unsteady loads experienced by the propellers of a CRP pair and rudder operating behind CRP and compare the levels of pressure pulses and radiated noise caused by CRP vs. single propeller.

2 PARAMETRIC DESIGN APPROACH

Compared to conventional open propellers, the hydrodynamic design procedures for CRP – whether shaft or podded – are less mature, and so are the performance extrapolation methods. Indeed, the CRP concept introduces additional variables in the design space such as the distribution of load and spacing between the forward and aft propellers, their respective number of blades and

ratio of propeller diameters. Since using contemporary transmission system propellers can be driven independently, the rates of revolution of the forward and aft propellers can also be optimized for best performance, depending on propulsor loading. Therefore, a simulation-driven design approach offers clear advantages in the solution of this multi-variable problem. Unlike the traditional simulation-based design where manually designed products are analyzed by CFD, and best candidates are chosen to meet the design criteria, the simulation-driven design method implies that many product variants are generated (semi-)automatically from repeated simulations, employing formal techniques of exploration and exploitation. This approach is already routinely applied in hull design (Harries et al. 2019; Ahmed et at. 2023), and it also finds its way in the design of propulsors and energy saving devices (Krasilnikov et al. 2019).

Within the innovation project for the Norwegian industrial sector IPN "ZeroCoaster", SINTEF Ocean were working on the task of designing an efficient propulsion system for a zero-emission coaster vessel. The overall ship design process is a multi-disciplinary problem which involves hydrodynamics (propulsion, maneuvering, seakeeping), cargo capacity, general arrangement, structural integrity, safety, logistics, environmental impact and CAPEX/OPEX analysis. Considering a tight interconnection between the designs of ship hull, propulsion system and steering system, the parametric model of the ship was developed in CAESES to accommodate these three components. As illustrated in Appendix 1, this model includes a partially parametric model of the ship hull and fully parametric models of the propeller(s) (blades and hub) and steering system (rudder and headbox). Partial parametrization of the hull uses as a starting point the CAD geometry of the hull prepared in a dedicated ship design software (e.g. NAPA) which is imported to CAESES. This model is then subject to transformations controlled by a set of parameters such as the hull's main particulars (LOA, B, H), design draft, waterline entrance (WL) angle, LCB, as well as the parameters describing shapes of the bulbous bow and stern tube. Some of these parameters are exposed in the design space as design variables. Transformations include simple scaling (for main particulars), curve delta shift (for draught/WL elevation), surface delta shift (for WL entrance angle), Lackenby shift (for LCB) and free form deformation (for the bow and stern tube shapes). The free form deformations are applied in predefined box volumes (shown in the figure in Appendix 1) that surround a part of the hull where the deformations apply. These deformations are controlled by the parameters that allow to modify length, height, width/radius and fullness of the surrounded body part. The stern tube shape is of immediate relevance to propeller design as it affects the position of the propeller with respect to hull, hub diameter and of course the inflow condition.

The models of the steering system (rudder and headbox) and propeller (blades and hub) are fully parametric. The rudder model implements a trapezoidal rudder configuration described by the chord length at the bottom and top ends, rudder height, elevation of rudder bottom above base, relative max thickness and position of the rudder axis in the axial and transverse directions. It supports an arbitrary user-defined profile of rudder sections. The same profile is also used for the rudder headbox, whose geometry is defined by a set of parameters like those of the rudder. In the present design, the high-efficiency rudder profile HSVA-MP71-10 was used. The propeller model is defined by conventional geometrical elements of blade cylindrical sections (chord length, max thickness, skew, rake, pitch, max camber), number of blades, position of propeller center, and parameters describing a conical hub with a boss cap. Separately, measurements are applied to control blade tip clearance at 12 o'clock, distance to base at 6 o'clock, distance between propeller plane and rudder leading edge, etc. These measurements are used to check the produced design candidates against constraints. The blade model is generated by the SINTEF Ocean propeller software AKPA which is used in the design process, and it is imported to CAESES as a CAD file. In the case of a CRP design, additional parameters are introduced to control the ratio between the diameters of the forward and aft propellers, distance between the respective propeller planes, and percentage load distribution between the propellers.

In the present work, the task of hull design was separate from the design of the propellers. The elaboration of hull lines was performed using a multi-variable optimization to meet the requirements of cargo capacity, general arrangement, cargo transportation logistics and cost-benefit analysis at the minimum possible power demand. At that stage, the effect of the propeller was considered approximately, using the open water diagrams of B-series propellers and propulsion factors estimated from the regression model in the software ShipX by SINTEF Ocean, which were subsequently corrected based on experience. The hull optimization resulted in recommended values of design ship speed V_S=9 (kn), design and ballast draughts T_{DWL}=6.3 (m) and T_{BWL}=4 (m), respectively, as well as a propeller diameter D=3.76 (m). It was decided that the same propeller diameter will be used in the design of the single propeller and the forward propeller of the CRP pair. The diameter ratio of CRP propellers D_{FRW}/D_{AFT}=0.9335 was established. These data were used as input to the propeller design workflow as illustrated in Appendix 2.

At the first step, the hull resistance calculation at the design draught and speed is repeated with a higher fidelity Scale Resolving turbulence modelling method (SRS). After that a preliminary self-propulsion calculation is performed using an Actuator Disk model to represent the effect of a working propeller. While more computationally expensive, the use of SRS simulation at

this early stage is justified by the need of more accurate information about the effective wake on propeller and propulsion factors (axial wake fraction, W_T, and thrust deduction factor, t). Besides, the said type of simulation is done only once for the given hull configuration, unless the wake pattern is judged undesirable, and new hull iterations are required.

The predicted values of propulsion factors and effective wake field are further used in the preliminary propeller design (PPD) and non-linear lifting-surface design calculation (AKPD) to elaborate optimum values of propeller RPM, obtain optimum loading distributions for flow-adapted propellers and derive distributions of blade sections' pitch and camber along the radius. The Generalized Optimum Condition (Achkinadze & Krasilnikov 1997) employed in the propeller design calculation considers both the axial and tangential components of the flow field, which is particularly important in the case of CRP design, and it also takes into account the effect of thrust deduction.

The blade pitch and camber distributions derived from the lifting surface calculation target maximum efficiency at the given operation conditions in the wake field. However, they can result in an impractical shape of the blade near the root and tip. Geometrical improvements in those areas, verification of propeller performance and cavitation characteristics in the effective wake are conducted at the next stage using the unsteady panel method calculation (AKPA). If found necessary, changes in chord length, skew, rake or thickness distributions are made, and the design calculations are repeated in an iterative manner. After that, the analysis code AKPA automatically prepares the geometry for CFD simulations of the propeller in open water and behind hull conditions. At this final stage of the design process, one may still perform elaboration of the hub design and introduce further corrections to the configuration of the blade tip to mitigate the strength of the tip vortex. Thus, new iterations may be required. CFD calculations are used to compute open water propeller characteristics, and to predict ship's self-propulsion performance with the designed propeller in full scale. For the prognosis of integral characteristics, the RANS method is normally sufficient. For a more accurate prediction of pressure pulses and radiated noise level, SRS simulations may again be employed.

3 VALIDATION OF NUMERICAL TOOLS

The simulation driven design workflow described in Section 2 relies on the use of propeller codes based on potential flow theory and automated templates for viscous CFD simulations. Careful validation, verification and calibration of these numerical tools is prerequisite for producing reliable designs. A detailed account of such studies is outside the scope of the present paper. Therefore, here we only provide some references to earlier works where such studies have been conducted and documented. Validation exercises with the panel method propeller code AKPA are found in (Achkinadze & Krasilnikov 2003) and (Achkinadze et al. 2003). The second reference contains the results for the cases of propeller-rudder interaction and podded CRP, which is of immediate relevance to the present problem. Recent validation examples with STAR-CCM+ CFD templates for open water, resistance and self-propulsion analyses can be found in (Koushan et al. 2020) and (Krasilnikov et al. 2023). Both the references include comparisons between full-scale CFD self-propulsion simulations, performance predictions based on model tests, and sea trial data. For the case of shaft CRP, detailed validation studies are conducted in (Johannessen et al. 2024). In this reference, a comparison between the CFD predictions of CRP open water characteristics and results of model tests from two testing facilities are presented, including total integral characteristics of the CRP pair, as well as thrust and torque of the forward and aft propellers.

4 RESULTS OF DESIGN EXPLORATION STUDY

In this section we describe the main finding from various steps of the propeller design process outlined in Section2, with the main focus on CRP design.

4.1 Hull resistance and nominal wake

Hull towing resistance simulations were performed using different turbulence modelling approaches, including the RANS method with the k-ω SST turbulence closure model, and the two Scale Resolving Simulation (SRS) techniques: Improved Delayed Detached Eddy Simulation (IDDES) (Shur et al. 2008), which incorporates a subgrid length-scale dependence on the wall distance, and Scale Resolving Hybrid (SRH) model (Duffal et al. 2019), which is a continuous hybrid RANS-LES technique using a special-temporal filtering, also known as the Hybrid Temporal Large Eddy Simulation. Both the said SRS methods use the k-ω SST turbulence model in the RANS branches of their solutions. The simulations were performed with the ship free to sink and trim, including the influence of surface roughness on the hull and rudder. A summarizing comparison of simulation results is presented in Table 1 for the design draught and speed. It can be observed that different methods predict close values of the resistance coefficient, Ct, and dynamic position of the ship. Larger differences are however found in the value of nominal wake fraction, W_{TN}. The time-average nominal wake fields predicted by different methods at the control section located x/D=0.15 in front of the propeller are shown in Figure 1.

Table 1. Results of towing resistance calculations using different turbulence modelling methods. T_{DWL}=6.3 (m), V_S=9 (kn)

Method	Ct	Sinkage	Trim	W_{TN}
RANS	0.00260	-0.0846	0.0986	0.312
IDDES	0.00269	-0.0841	0.0975	0.320
SRH	0.00261	-0.0845	0.0931	0.330

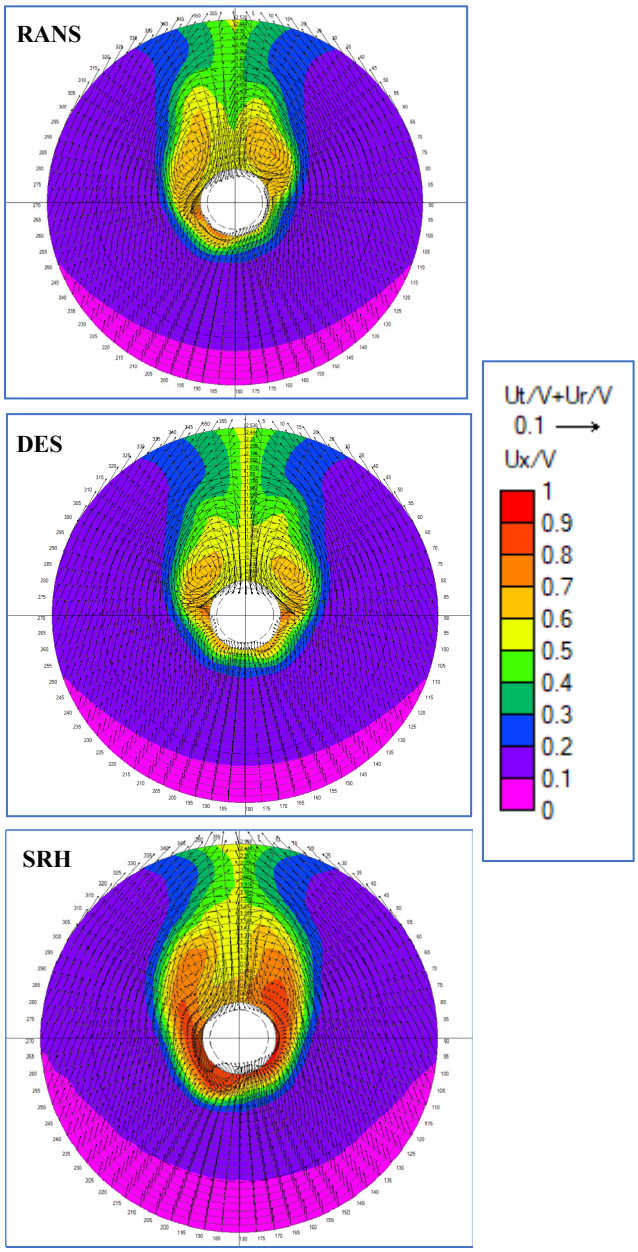

Figure 1: Nominal wake field predicted using different turbulence modelling methods. T_{DWL}=6.3 (m), V_S=9 (kn)

The SRS methods, and especially SRH, predict larger flow deficit in the hull wake, and they provide a better resolution of the zones of separated flow. It has to be noted that time-depended wake pictures predicted by IDDES and SRH are quite unsteady, showing that the mentioned separation zones present the assemblies of vortices of different scales which participate in mutual interaction.

4.2 Estimation of propulsion factors

For the estimation of propulsion factors to be used in the propeller design calculation a simplified self-propulsion simulation was performed using an Actuator Disk (AD) model of the propeller. The AD model assumes a standard optimum distribution of propeller loading, and the thrust produced by the disk is adjusted until it balances ship resistance with operating propeller. The velocity field induced by the disk is obtained from an additional simulation of the same AD in open water condition where the inflow speed is estimated using the relationships of momentum theory, so that the disk produces the same thrust (and, hypothetically, the same field of induced velocity) as in behind hull conditions. This self-propulsion calculation was performed using the SRH turbulence model, and it resulted in the following estimations of the effective axial wake fraction and thrust deduction factor: W_T=0.273, t=0.218. These values can be compared with the estimation obtained from the regression model of ShipX which uses the ship type and its main particulars as input: W_T=0.280, t=0.200. The numerical prediction appears to be quite close to the database value. For comparison, the same self-propulsion simulation done with the RANS method shows lower values of propulsion factors: W_T=0.252, t=0.190. The picture of effective wake at the control section is shown in Figure 2.

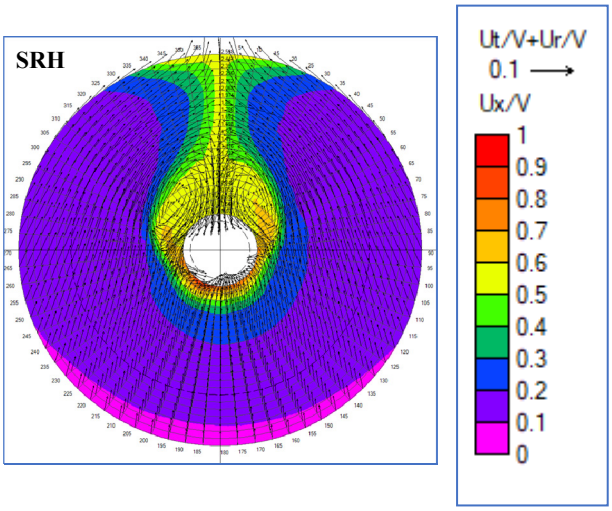

Figure 2: Effective wake field predicted from simplified self-propulsion calculation using the SRH turbulence model. T_{DWL}=6.3 (m), V_S=9 (kn)

Comparing this image with the nominal wake shown in Figure 1, one can observe typical changes in the effective wake field which are due to flow acceleration by the propeller – lower flow deficit, reduction of separation zones, and overall inward contraction of the wake. In the present design study, it was assumed that the axial wake fraction and thrust deduction factor should be comparable for the cases of single propeller and CRP designed from the same thrust loading condition, an hypothesis which was later verified by CFD propulsion analyses with fully resolved propellers. Further, the same effective wake field was used as input to the design calculation of both the single propeller and CRP.

4.3 Wake adapted propeller design

The propellers were designed to provide the required total thrust of T_P=110.75 (kN), at the given diameters of propellers: D=3.76 (m) for the single propeller, and D_{FRW}=3.76 (m), D_{AFT}=3.51 (m) for the CRP, in the given effective wake field. The propeller RPM was subject to optimization using the lifting-line module of the design code AKPD. In the case of CRP, optimization of load distribution and distance between the propellers was also performed. The forward and aft propellers of the CRP pair have 4 and 5 blades, respectively.

Figure 3 shows the open water efficiency and propulsive efficiency of the single propeller as functions of RPM. The RPM=100.1 is chosen for the blade design.

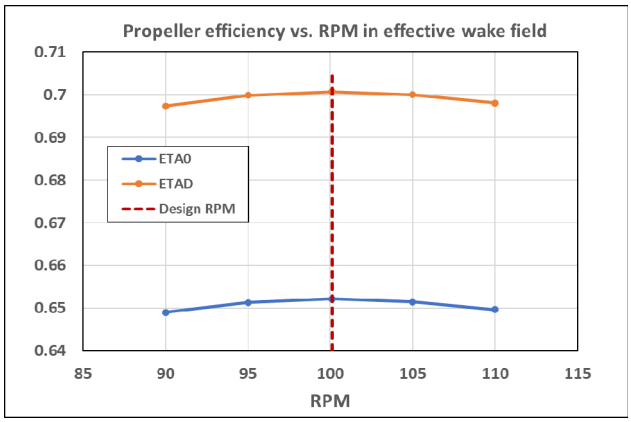

Figure 3: Optimization of single propeller RPM in effective wake field

The optimization exercise with load distribution between the propellers of the CRP pair results in dependencies presented in Figure 4. Maximum efficiency is achieved at a thrust distribution 60/40 % between the forward and aft propellers, and the corresponding values of RPM are 79.35 and 70.1, the RPM ratio being n_{FRW}/n_{AFT}=0.8834.

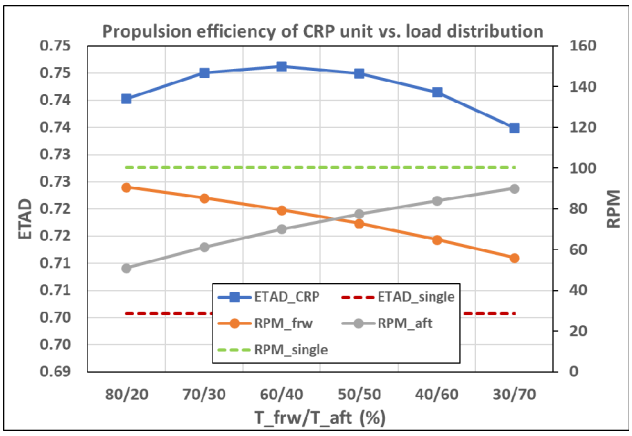

Figure 4: Variation of propulsive efficiency and RPM of CRP with thrust load distribution between the forward and aft propellers, x_{dPP}/D_{FRW}=0.195

The results shown in Figure 4 correspond to the distance between the CRP propellers being equal to x_{dPP}/D_{FRW}=0.195. The studies done with the lifting-line design code indicate that propulsive efficiency of CRP increases slightly as the distance between the propellers is reduced, as illustrated in Figure 5. It should be noted that these estimations are obtained without the effect of blade thickness included. Reducing the separation between propellers below 0.16 was found impractical for construction reasons, and for the final design the value of x_{dPP}/D_{FRW}=0.175 was accepted. Comparing the values of propulsive efficiency predicted by the design code, it can be concluded that a power reduction of about 7.0% may be expected due to CRP at the given design condition.

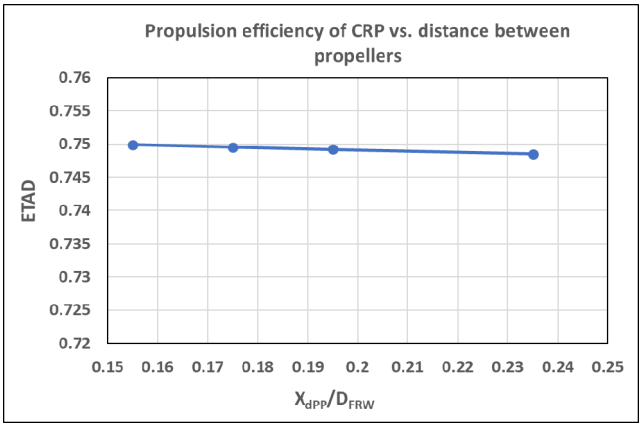

Figure 5: Influence of the distance between propellers on propulsive efficiency of CRP

With the distance and thrust distribution between the propellers, and respective values of RPM established, the radial distributions of pitch and maximum camber are obtained from the non-linear lifting-surface calculation.

4.4 Design verification by panel method

The geometry resulting from the lifting-surface design calculation requires a number modifications to consider practical requirements of blade manufacturing and local blade strength. In the present case, modifications primarily concerned the distributions of camber near the blade root and blade tip, as well as local values of section thickness near the leading and trailing edges. The final pitch and camber distributions of the forward and aft propellers of the CRP pair are shown in Figures 6 and 7, respectively. The aft propeller has a higher pitch and lower maximum camber as a result of its design adaptation to operation in the swirled slipstream of the forward propeller. Increased values of camber towards the blade root are the result of design adaptation to the wake field behind the ship hull, and for the aft propeller, it also reflects the influence of slipstream swirl. Since propeller blades feature a moderate amount of skew (23.5° for the forward propeller, and 29.0° for the aft propeller), some rake distribution was also applied

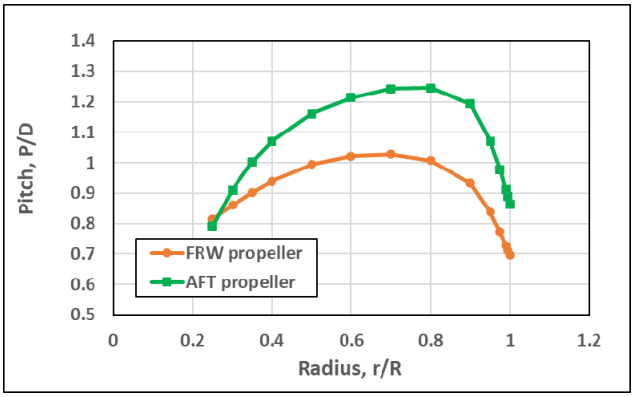

Figure 6: Radial pitch distribution of CRP propellers

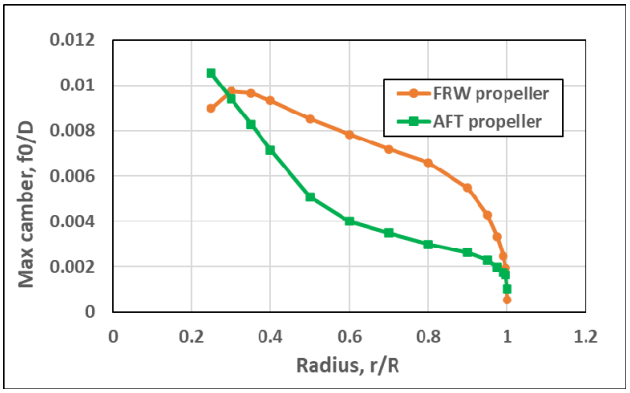

Figure 7: Radial camber distribution of CRP propellers

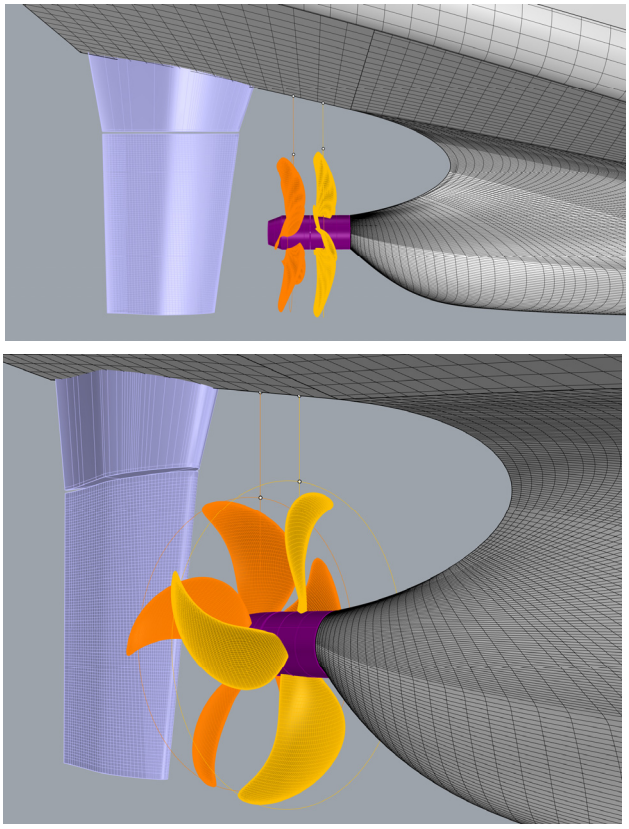

Figure 8: Arrangement of the CRP propulsion system

to maintain distance between propeller blades and to increase the tip clearance with respect to the ship hull. The tip clearance values are equal to 0.265D for the forward propeller and 0.363D for the aft propeller. The final geometry of the designed CRP and their arrangement at the aftship are illustrated in Figure 8. This figure also shows the propeller hubs with a conical downstream cap and the rudder with the headbox designed for the present vessel. The described modification in blade geometry is the result of panel method analysis calculations where the distribution of pressure over the blades and level of pressure fluctuations on the hull were monitored along with the integral characteristics of the propellers.

A comparison of CRP performance characteristics predicted by the design (lifting-surface) and analysis (panel method) calculations in the effective wake field is presented in Table 2. This table also contains the results of final design verification by CFD self-propulsion simulations which is discussed in Section 5. Herewith, we focus on the comparison between the design and analysis codes. It can be concluded that the analysis calculation performed in the non-uniform effective wake field confirms very well the prognosis given by the design code regarding the total performance of CRP as well as thrust and torque of individual propellers. Certain differences between these calculations can of course be expected due to: (i) different numerical formulations; (ii) use of circumferential average wake in the design calculation; (iii) modifications in final blade geometries which are used in the analysis calculation.

Table 2: CRP performance characteristics predicted at different stages of the design process. T_{DWL}=6.3 (m), V_S=9 (kn)

	Design	Analysis	CFD S-P
n_frw	79.35	79.35	79.8
KTP_frw	0.18526	0.18834	0.1978
KQP_frw	0.028942	0.03016	0.03235
n_aft	70.1	70.1	70.5
KTP_aft(frw)	0.123506	0.12205	0.1102
KQP_aft(frw)	0.021248	0.02065	0.01703
KTP	0.308766	0.31039	0.308
KQP	0.05019	0.05081	0.04938
TP (kN)	110.75	111.33	111.73
PD (kW)	534.69	542.44	540.19
ETAD	0.7495	0.7426	0.7418
T_frw (%)	60.00	60.68	64.22
T_aft (%)	40.00	39.32	35.78

Figure 9 shows the cavitation margins on propeller blades predicted by the unsteady panel method calculations. These calculations were done for the conditions of ballast draught T_{BWL}=4 (m) which pose a higher risk of cavitation. For comparison, the results are also presented

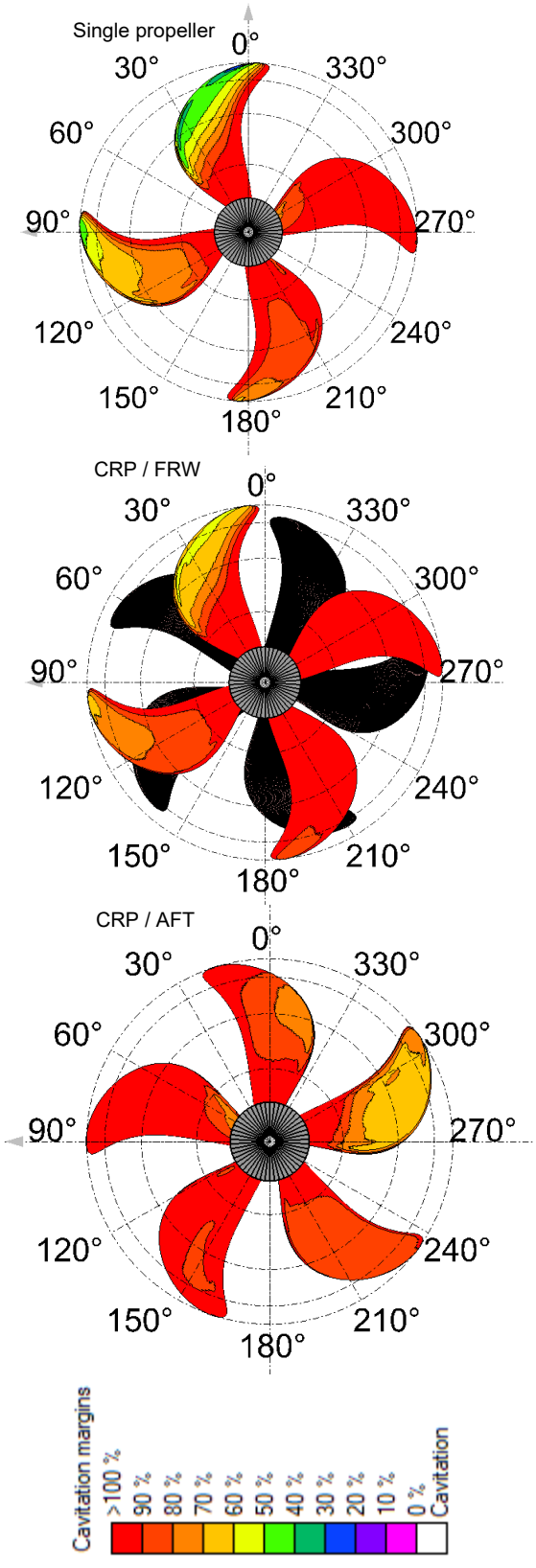

Figure 9: Cavitation margins on propeller blades in ballast conditions. T_{BWL}=4.0 (m), V_S=9 (kn)

for a single propeller design. It can be noticed that due to the reduction of propeller loading, cavitation margins on the suction side of the forward propeller of the CRP pair are significantly larger compared to the single propeller design. Because the aft propeller was designed to operate in the slipstream of the forward propeller, it also shows sufficiently large cavitation margins in the design conditions.

5 FINAL PERFORMANCE ANALYSIS

To perform a final verification of the propeller designs and quantify power savings achieved with the CRP solution against a single propeller, CFD self-propulsion simulations were carried out for a range of ship speeds. Because of heavier computation effort required, these simulations were done with the RANS method only, which may naturally influence the comparison with earlier potential calculations done in the wake field predicted from the SRH simulation. It is however logical to assume that the differences in performance of the CRP and single propeller would be comparable regardless of the turbulence modelling approach. The computation mesh used in self-propulsion calculations with CRP consisted of 37.3 million cells, of which 12.8 million cells were in the main fluid region, while remaining cells were distributed approximately equally between the rotating regions of the forward and aft propellers. Simulations were done with the free surface, using the wall functions approach, and the wall Y+ values were in average around 120 on the ship hull and 60÷70 on propeller blades, rudder and headbox. The time step in the Sliding Mesh calculation phase corresponded to 2° of rotation of the forward propeller. To find the self-propulsion point, propeller RPM was adjusted until propeller thrust compensated ship resistance (including 15 % sea margin and additional resistance components such as bilge keels and tunnel thruster resistance) with the accuracy of 0.5 %. In the case of CRP, the ratio between the RPM of the forward and aft propellers was kept constant and equal n_{FRW}/n_{AFT}=0.8834 as set in the design task. This RPM ratio remained the same in the calculations at different ship speeds.

The CRP performance characteristics found from the self-propulsion calculation at the design speed are given in Table 2, column "CFD S-P". The computed values of total propeller thrust, T_P, and shaft delivered power, P_D, are found to be very close to the predictions by the analysis code in the effective wake. However, the predicted values of RPM are about 0.6% higher than those used in the design. The propulsion calculation also shows a slightly different thrust distribution between the propellers, where the first propeller appears about 4% heavier loaded, and the after propeller 4% lighter loaded than in the design specification. The mentioned deviations are attributed to the differences in the wake field due to turbulence modelling approach, as well as viscous interaction effects taking place between the propellers, hull and rudder, which can neither be captured in potential calculations nor completely included in the effective wake derived from the simulations with the Actuator Disk model.

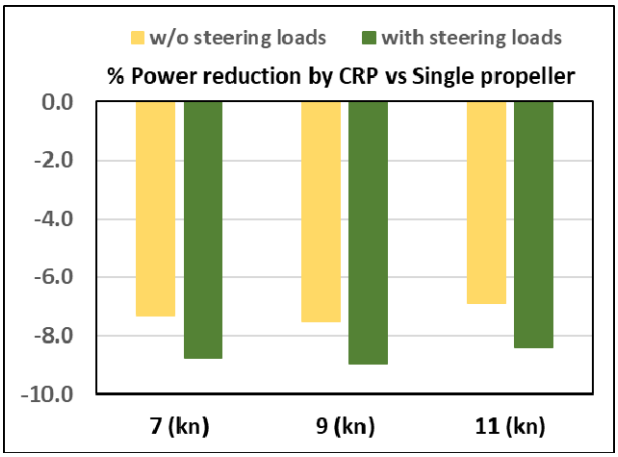

Figure 10: Reduction of shaft delivered power, P_D, achieved with CRP compared to single propeller

The comparison between propulsion performance of the ship equipped with the CRP and single propeller shows a reduction in required shaft delivered power achieved with CRP as presented in Figure 10. In this figure, the yellow bars correspond to self-propulsion calculations with the rudder installed at 0°, and they indicate power reduction of (7÷7.5) % for the ship equipped with CRP. As illustrated in Figure 11, in the case of a single propeller, the rudder resistance is lower than with CRP, which is explained by the action of the lift force produced by the rudder operating in the field of tangential velocity induced by the propeller. However, the same lift also results in a larger side force acting on the rudder, which needs to be compensated by a rudder angle to keep the ship on a straight course. The average side force acting on the rudder behind CRP is very close to zero, although its time history reveals larger oscillations. Further, an action of the rudder is required to balance the effect of slipstream precession of the single propeller. The mentioned effects would result in additional resistance of the ship, so that with the steering loads included in the analysis the power reduction by CRP is estimated to be at the level of (8.5÷9) % compared to the single propeller (shown by green bars in Figure 10).

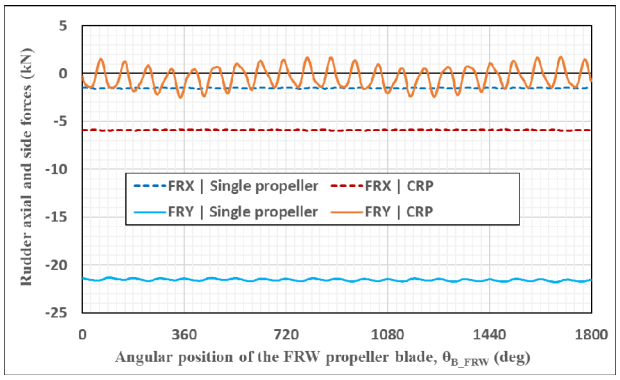

Figure 11: Forces acting on the rudder behind CRP and single propeller recorded during 5 propeller revolutions

The highest power savings are achieved at the design speed. However, the differences between the three speeds considered in the simulation are quite small. At off-design conditions, the efficiency of the CRP system can potentially be improved by the adjustment of RPM of the forward and aft propellers.

In Figure 12, we compare the distributions of kinetic energy associated with the tangential velocity component in the flow around the aftship. One can see that, in the case of CRP, the tangential velocity in the propeller slipstream is nearly zero which confirms that the aft propeller completely utilized the rotational energy lost by the forward propeller. The effect of slipstream precession is also visible for the ship with single propeller, whereas in the case CRP the slipstream is aligned with the propeller shaft.

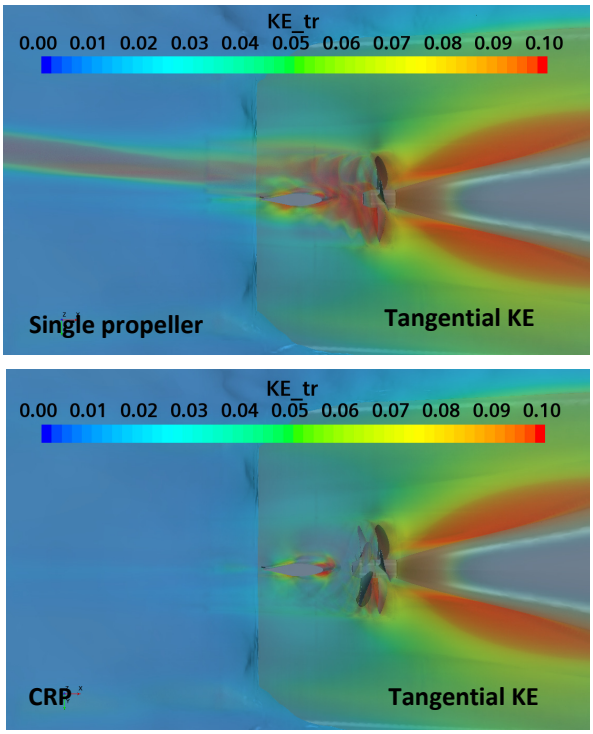

Figure 12: Field of tangential kinetic energy in the flow around aftship with the CRP and single propeller. T_{DWL}=6.3 (m), V_S=9 (kn)

From the operation standpoint, it is important to assess the magnitude of unsteady loads which act on individual propeller blades, and which are transmitted to the shaft and bearings. In Figure 13, the time histories of one blade thrust acting on the single propeller and CRP are presented for the 5 propeller revolutions along with a comparison of maximum blade thrust amplitudes. The blades of the forward and aft propellers of the CRP pair experience slightly higher amplitudes of thrust variation compared to the single propeller case. Higher frequency thrust oscillations of small amplitudes are also evident due to interaction between the vortex systems of the two propellers.

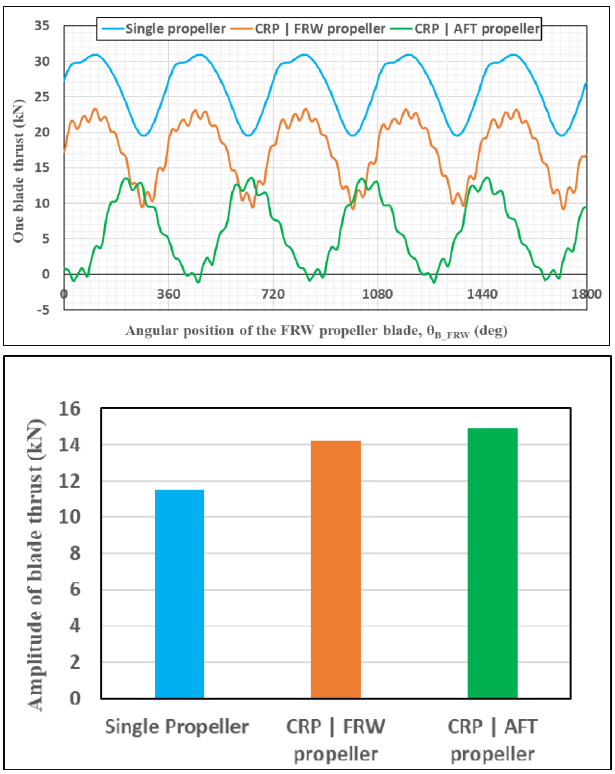

Figure 13: Time histories and maximum amplitudes of one blade thrust for the CRP and single propeller. T_{DWL}=6.3 (m), V_S=9 (kn)

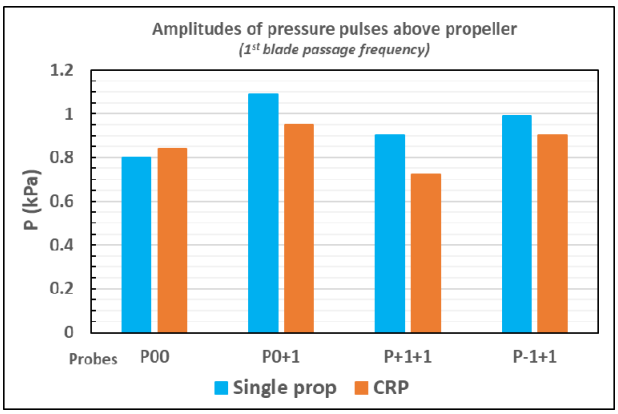

Figure 14: Amplitude of pressure pulses above propeller. T_{DWL}=6.3 (m), V_S=9 (kn)

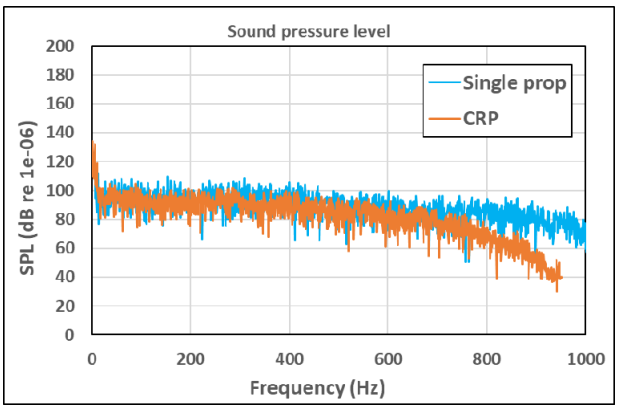

Figure 15: Levels of noise radiated by the CRP and single propeller. T_{DWL}=6.3 (m), V_S=9 (kn)

Finally, we conducted the simulation to predict pressure pulses on the ship hull and sound pressure levels emitted by the CRP and single propeller at the design conditions. Since this type of analysis required more accurate resolution of the anisotropic field of turbulence, the propulsion calculation was continued at the found (and now fixed) propeller RPM using the IDDES method. No additional mesh refinement was however made. A sufficient number of propeller revolutions was allowed to ensure convergence of pressure monitors at the control points and to accumulate statistical data. The calculation of radiated noise was performed using the method of acoustic analogy, according to the Ffowcs Williams-Hawkings method with a permeable control surface (P-FWH) (Krasilnikov et al. 2022). The results are summarized in Figures 14 and 15, respectively, for the pressure pulses and noise levels. Overall, the CRP design shows reduced levels of pressure fluctuations on ship hull and lower radiated noise at higher frequencies in the simulated non-cavitating conditions of the design draft. Under the conditions of increased risk of cavitation, the benefits of CRP will be even more pronounced due to reduced load on propellers and larger cavitating margins.

5 CONCLUSIONS

A simulation driven design involving connection between numerical tools of different fidelity levels is shown to be a robust and accurate approach to the development of efficient propulsion systems for modern ships such as flow-adapted counter-rotating propellers (CRP). Fast potential propeller codes are an essential part of the design procedure as they permit exploration of a large design space within a short time. High-fidelity CFD tools allow for an adequate prognosis of the inflow on the propulsor and the ship's propulsion performance under realistic operation conditions in full scale.

It is demonstrated that a power reduction of up to (8.5÷9.0) % can be achieved in the range of speeds around the design point with a flow-adapted CRP solution compared to a single propeller designed for the same conditions. The vessel equipped with a CRP is also expected to have superior manoeuvring performance.

The blades of the forward and aft propellers of a CRP pair experience slightly higher amplitudes of thrust variation compared to the single propeller case. Higher frequency thrust oscillations of small amplitudes are also evident due to interaction between the vortex systems of the two propellers. Compared to the case of a single propeller, a rudder operating behind CRP shows a higher resistance, but a considerably lower side force. Both the results are due to the negation of swirl in propeller slipstream by the action of the aft propeller.

The CRP design shows reduced levels of pressure fluctuations on the ship hull and lower radiated noise at higher frequencies at non-cavitating conditions of the design draft. Even greater benefits are expected in the conditions with a higher risk of cavitation such as ballast.

REFERENCES

Achkinadze, A.S., Berg, A., Krasilnikov, V.I. & Stepanov, I.E. (2003). 'Numerical Analysis of Podded and Steering Systems Using a Velocity Based Source Boundary Element Method with Modified Trailing Edge'. Proceedings of the Propellers/Shafting'2003 SNAME Symposium, Virginia Beach, VA, USA, September 17-18.

Achkinadze, A.S. & Krasilnikov, V.I. (1997). 'A Generalized Optimum Condition for Wake Adapted Screw Propeller'. Proceedings of the Propellers/Shafting'97 SNAME Symposium, Virginia Beach, VA, September 23-24.

Achkinadze, A.S. & Krasilnikov, V.I. (2003). 'A New Velocity Based BEM for Analysis of Non-cavitating and Cavitating Propellers and Foils.' Oceanic Engineering International, 2003, 7(1): 33-47.

Ahmed, O., Godfrey, A., Harries, S., & Wheeler, M. (2023). 'Parametric design and optimization of planing hull; a comparison of optimization methods'. Proceedings of the 25th Numerical Towing Tank Symposium NuTTS 2023, 15 – 17 October, Ericeira, Portugal.

Carlton, J.S. (2007). 'Marine propellers and propulsion'. 2nd ed., Butterworth-Heinemann.

Duffal, V., de Laage de Meux, B. &Manceau, R. (2019). 'Development and validation of a hybrid RANS-LES approach based on temporal filtering'. Proceedings of the 8th Joint Fluids Engineering Conference, San Francisco, CA, USA, 28 July–1 August.

Flippone, A. (2023). ' Historical development of the coaxial contra-rotating propeller'. The Aeronautical Journal, 127, pp.699-736

Harries, S., Dafermos, G., Kanellopoulou, A., Florean, M., Gatchell, S., Kahva, E., & Macedo, P. (2019). 'Approach to Holistic Ship Design – Methods and Examples'. Computer Applications and Information Technology in the Maritime Industries (COMPIT 2019), March, Tullamore, Ireland.

IHI (1993). 'IHI CRP System for Large Merchant Ships'. Ship Technology International'93, SPG, 1993.

ITTC (2008). 'The Specialist Committee on Azimuthing Podded Propulsion. Final Report and Recommendations to the 25th ITTC'. Proceedings of the 25th ITTC – Volume II, Fukuoka, Japan.

Jukola, H. & Ronkainen, T. (2006). 'Contra-Rotating Propellers – Combination of DP Capability, Fuel Economy and Environment'. Proceedings of the Dynamic Positioning Conference, Houston, USA, October 17-18.

Koushan, K., Krasilnikov, V.I., Nataletti, M., Sileo, L. and Spence, S. (2020). 'Experimental and Numerical Study of Pre-Swirl Stators PSS'. Journal of Marine Science and Engineering, 2020, 8, 47.

Krasilnikov, V.I., Koushan, K., Nataletti, M., Sileo, L., & Spence, S. (2019). 'Design and Numerical and Experimental Investigation of Pre-Swirl Stators PSS'. Proceedings of the 6th International Symposium on Marine Propulsors smp'19, May, Rome, Italy.

Krasilnikov, V.I., Savio, L., Koushan, K., Felli, M., Abdel-Maksoud, M., Kimmerl, J., Reichstein, N., Fageraas, A. & Sun, J. (2022). 'Towards Reliable Prediction of Propeller Noise: Challenges and Findings of the Project ProNoVi'. Proceedings of the 7th International Symposium on Marine Propulsors smp'22, October, Wuxi, China.

Krasilnikov, V.I., Skjefstad, V.S., Koushan, K. & Rambech, H.J. (2023): 'A Calibration Study with CFD Methodology for Self-Propulsion Simulations at Ship Scale', Journal of Marine Science and Engineering, 2023, 11, 1342.

Mewis, F. (2014). ' Six Years Mewis Duct® - Six Years of Hydrodynamic Development'. Schiffbautechnische Gesellschaft Fachausschuß Schiffshydrodynamik Sprechtag "Energy-Saving Devices", Hamburg, October 9.

Quereda, R., Sobrino, M.P., Gonzalez-Adalid, J. & Soriano, C. (2019). 'CRP propulsion system for merchant ships. Past, present and future'. Proceedings of the 6th International Symposium on Marine Propulsors smp'19, May, Rome, Italy.

Ship Technology. (2014). 'MV Juanita Platform Supply Vessel'. August 10, https://www.ship-technology.com/projects/mv-juanita-platform-supply-vessel/?cf-view.

Shur, M.L., Spalart, P.R., Strelets, M.K. & Travin, A.K. (2008). 'A hybrid RANS-LES approach with delayed-DES and wall-modelled LES capabilities'. Int. J. Heat Fluid Flow, 2008, 29, 1638–1649

APPENDIX 1. Parametric CAD model of ship hull, propulsion and steering systems in CAESES

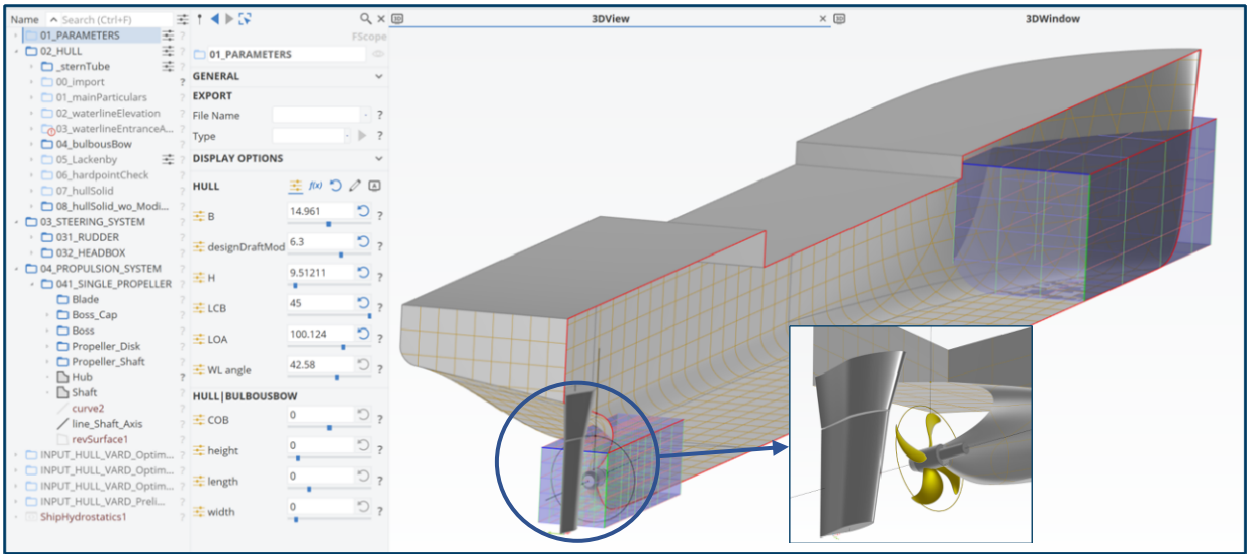

APPENDIX 2. Propeller design workflow and software connection